AIP | Physics of Fluids

Effect of unequal cylinder spacing on vortex streets behind three side-by-side cylinders

H. J. Zhang and Y. Zhou

Citation: Phys. Fluids **13**, 3675 (2001); doi: 10.1063/1.1412245

View online: http://dx.doi.org/10.1063/1.1412245

View Table of Contents: http://pof.aip.org/resource/1/PHFLE6/v13/i12

Published by the American Institute of Physics.

Effect of unequal cylinder spacing on vortex streets behind three side-by-side cylinders

H. J. Zhang and Y. Zhou
Department of Mechanical Engineering, The Hong Kong Polytechnic University, Hung Hom, Kowloon, Hong Kong

(Received 20 December 2000; accepted 27 August 2001)

The turbulent near-wake of three side-by-side circular cylinders with equal or unequal spacing has been experimentally investigated using various techniques, including the hot wire, laser Doppler anemometer, and flow visualization. The work aims to understand the effect of unequal cylinder spacing on the vortex streets behind the three cylinders. When the cylinder center-to-center spacing is identical, i.e., $T_1/d = T_2/d = 1.5$, the flow is symmetric about the centerline, with one wide wake behind the central cylinder and one narrow wake on each side of the wide wake. The dominant frequency in the narrow wakes is about 5.4 times that in the wide wake. The observation is consistent with previous reports, thus lending credence to the present measurement. As T_2/d is slightly increased to 1.6, a remarkable change occurs in the flow. A comparison is made between the cases of equally and unequally spaced cylinders in terms of the pressure around the cylinders, drag, lift, dominant frequencies, and vortex formation mechanisms. The flow topology (vortex patterns) and downstream evolution are also discussed in detail. © *2001 American Institute of Physics.* [DOI: 10.1063/1.1412245]

I. INTRODUCTION

Flows around multiple cylinders have received considerable attention in the past because of its inherent importance and practical significance in many branches of engineering.[1] It is not uncommon that engineering structures are immersed in the wake of multiple structures, for example, the blades of multistage turbo-machines, tube bundles in heat exchangers, marine structures, a group of tall buildings, and chimneys. It is therefore important to understand the flow patterns and aerodynamic characteristics behind multiple bluff bodies in order to estimate gust-wind effects and aerodynamic forces on downstream structures or to determine the heat transfer of cross-flow heat exchangers.

Flow behind two side-by-side circular cylinders has been investigated extensively, which improves our understanding tremendously.[2–9] It is now well established that when the cylinder center-to-center spacing ratio T/d is less than 1.2, the two cylinders act like a single bluff body, forming a single Kármán vortex street. For $T/d \approx 1.2-2.2$, the gap flow between the cylinders is deflected, thus generating one narrow and one wide wake. The deflected gap flow is bi-stable, that is, the deflection can change its direction in a random way and stay in the same direction for a while. Two dominant frequencies have been identified. The higher and lower frequencies are associated with the narrow and wide wakes, respectively. For $T/d > 2.2$, two coupled vortex streets occur.

The flow behind three side-by-side circular cylinders bears similarity in many aspects, such as multiple dominant frequencies and the gap flow deflection and flopping, to the two side-by-side cylinders. This flow is, however, more complicated. For example, there are two gap flows that may deflect in different ways and more types of flow patterns involved. Evidently, this flow is more representative of those behind a row of circular cylinders; many of its features are shared by the latter.[10–12] Kumada *et al.*[13] measured the pressure distributions, velocity distributions and vortex shedding frequencies of a three side-by-side cylinder wake at the Reynolds number $\mathrm{Re} = (1.0-3.2)\times 10^4$. Four typical flow regimes were identified. When T/d was between 1.0 and 1.125, the three cylinders behaved like a single bluff body and one vortex street occurred. For $T/d = 1.125-1.35$, both gap flows between the cylinders deflected towards one side, thus forming narrow and wide wakes. For $T/d = 1.35-2.225$, the two gap flows were deflected towards the free-stream, respectively. Consequently, two narrow wakes occurred behind the two outer cylinders and one wide wake behind the central one; the narrow and wide wakes are associated with high and low dominant vortex frequencies, respectively. The two outer cylinders also had large drag, compared with the central cylinder. One distinct difference of the three-cylinder flow from that of two cylinders was that the gap flow was generally quasi-stable, unless near $T/d = 2.225$ where the gap flow deflection might change its direction. For $T/d = 2.225-3.75$, three separate vortex streets were seen. The flow behind three side-by-side plates behaved quite similarly.[14] Guillaume and LaRue[15] observed for $\mathrm{Re} = 2500$ three quasi-stable modes for $T/d = 1.338-1.730$, one quasi-stable mode with forced flopping for $T/d = 1.730-1.850$, and only one quasi-stable mode for $T/d = 1.850-2.202$. More recently, Sumner *et al.*[8] measured the flow patterns behind two and three side-by-side circular cylinders in a range of $T/d = 1-6$ for $\mathrm{Re} = 500-3000$ using flow visualization and particle image velocimetry (PIV). They noted considerable variation in the reported flow patterns at a given T/d. Using a combination of an X-wire and a cold

wire, Zhou *et al.*[9] measured the velocity and temperature fluctuations at Re=1800 in the two- and three-cylinder wakes. They observed that the cross-stream distributions of the Reynolds stresses and heat flux varied significantly, which was ascribed to different flow patterns, as T/d reduced from 3.0 to 1.5.

Previous studies on multiple side-by-side bluff bodies have mostly focused on the identical bluff bodies of the same spacing. However, engineering structures may be arranged in a more complicated way, for example, different bluff bodies, unequal spacing, or in the staggered configuration. Palmer and Keffer[16] measured an asymmetric turbulent wake generated by two side-by-side cylinders of unequal diameter at different downstream distances from the cylinders. Their aim was to create and investigate the region of turbulent ''energy reversal'' where the turbulent kinetic energy production turns negative. Sumner *et al.*[17] measured the flow patterns of two cylinders in a staggered arrangement. They observed nine flow patterns and found that vortex shedding frequencies were more properly associated with individual shear layers rather than with cylinders. However, to our knowledge, the effect of unequal spacing on the flow has not been well documented in the literature. Therefore, a number of questions have yet to be answered. How would drag and lift on individual cylinders be affected by the unequal spacing between three side-by-side cylinders? How many dominant vortex frequencies could occur? Furthermore, how would the flow patterns and their downstream evolution be affected?

This work aims to investigate the effect of unequal spacing on the flow behind three side-by-side cylinders. To this end, velocity fluctuations were obtained at $10d$ from the cylinder for equal and unequal cylinder spacing using two X-wires, with one fixed to provide a reference phase and the other moving across the wake. A phase averaging technique is used to extract typical flow topology (vortex pattern) in the near-wake from the velocity data. The vortex formation and downstream evolution in each case were investigated in detail based on the measured pressure around cylinders, velocity measurements in the close vicinity of cylinders, streamwise variation of dominant frequencies, and laser-illuminated flow visualization.

II. EXPERIMENTAL DETAILS

Most experiments were carried out in a closed circuit wind tunnel with a square cross-section ($0.6\times0.6\,\mathrm{m}^2$) of 2.0 m length, including fluctuating velocity measurements using hot-wire and laser Doppler anemometer (LDA) techniques and pressure measurements around cylinders. Three brass cylinders of 0.0127 m diameter were installed side-by-side in the mid-plane and spanned the full width of the working section (Fig. 1). The cylinders were located at 0.2 m downstream of the exit plane of the contraction. This resulted in a maximum blockage of about 6.3% and an aspect ratio of 47. The transverse spacing T_1/d between the central and lower cylinders was fixed at 1.5 and T_2/d between the central and upper cylinders was varied from 1.5 to 3.0. Detailed measurements were performed with respect to two configurations, that is, $T_1/d=T_2/d=1.5$ (symmetric arrangement) and $T_1/d=1.5$, $T_2/d=1.6$ (asymmetric arrangement).

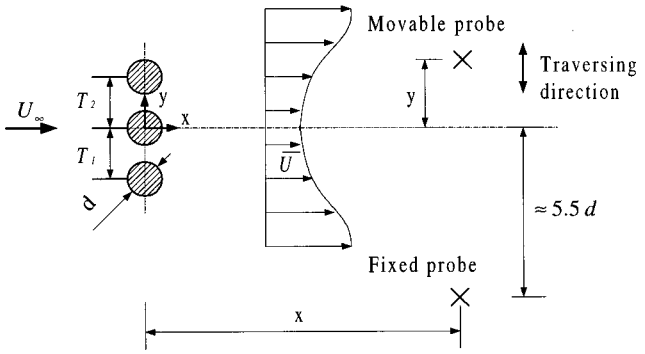

FIG. 1. Experimental arrangement.

A. Pressure, lift, and drag measurements

One of the three cylinders was instrumented at the mid-span position with a single wall pressure tap of 0.5 mm in diameter. A pressure transducer was connected to the tap to measure the wall static pressure. The cylinder was rotated at an interval of 5° to give the angular distribution of wall static pressure around the cylinder surface. The mean drag and lift on the cylinder were evaluated by integrating the wall mean pressure around the cylinder. In this article, unless otherwise stated, the flow was measured at Re ($\equiv U_\infty d/\nu$, where U_∞ is the free stream velocity and ν is the kinematic viscosity) $=5800$. Measurements were also carried out on a single cylinder at the same Re as the three-cylinder case so as to provide a baseline for evaluating the effects of unequal spacing between cylinders on the flow.

B. Hot-wire measurements

While a movable X-wire probe was used to measure the streamwise and lateral velocity fluctuations u and v, another fixed X-wire, located at $5.5d$ below the center of the central cylinder ($y=0$), was used to provide a phase reference for the signals from the movable X-wire. Measurements were conducted at $x/d=10$, where x is the streamwise distance measured from the cylinder center. In order to monitor the downstream evolution of vortices, single hot-wire data was obtained at $y/d=3.0$ and $x/d=1.6$, 2.2, 2.8, 3.6, 4.4, and 5.2 for spectral analysis. In the free-stream, the longitudinal turbulence intensity was measured to be approximately 0.4%. The hot wires were operated with constant temperature circuits at an overheat ratio of 1.8. Signals from the circuits were offset, amplified, and then digitized using a 16-channel (12-bit) A/D board and a personal computer at a sampling frequency $f_{\mathrm{sampling}}=3.5\,\mathrm{kHz}$ per channel. The duration of each record was 20 s.

C. LDA measurements

In order to obtain the quantitative information on the flow field at a close vicinity downstream of the cylinders, measurements have also been made at $x/d=2.5$ in the wind tunnel with a two-component LDA (Dantec Model 58N40

two-component LDA with enhanced FVA signal processor). The measuring volume has a minor axis of 1.18 mm and a major axis of 2.48 mm. Thus, the measured mean velocity was estimated to have an error of less than 3% and the corresponding error for the measured root mean square value was less than 10%. The seeding of the flow was provided by smoke generated by a Dantec SAFEX 2010 fog generator from Dantec fog fluid (standard). The LDA system comes with the software for data processing and analysis. Therefore, in addition to the mean field, the data could also be processed to yield information on the Reynolds stresses in the plane of mean shear.

D. Laser-illuminated flow visualization in water tunnel

Flow visualization was carried out in a water tunnel with a square working section ($0.15\times0.15\,m^2$) of 0.5 m length. Three side-by-side acrylic circular tubes with identical diameters of 0.01 m were horizontally mounted 0.2 m downstream of the exit plane from the tunnel contraction. The blockage was 20%. For each cylinder, dye (Rhodamine 6G 99%, which has a faint red color but becomes metallic green in color when excited by laser) was introduced through injection pinholes located at the mid-span of the tube. A thin laser sheet, which was generated by laser beam sweeping, provided illumination vertically at the mid-plane of the working section. The laser beam was provided by a Spectra-Physics Stabilite 2017 Argon Ion laser source with a maximum power output of 4 W. The flow motion was recorded with a digital video camera recorder (Sony DCR-PC100E). The video camera has a framing rate of 25 frames per second. The real time index is provided for each frame. For the flow visualization, Re was 150–2000. At a larger Re, the dye diffused too rapidly to be an effective marker of vortices.

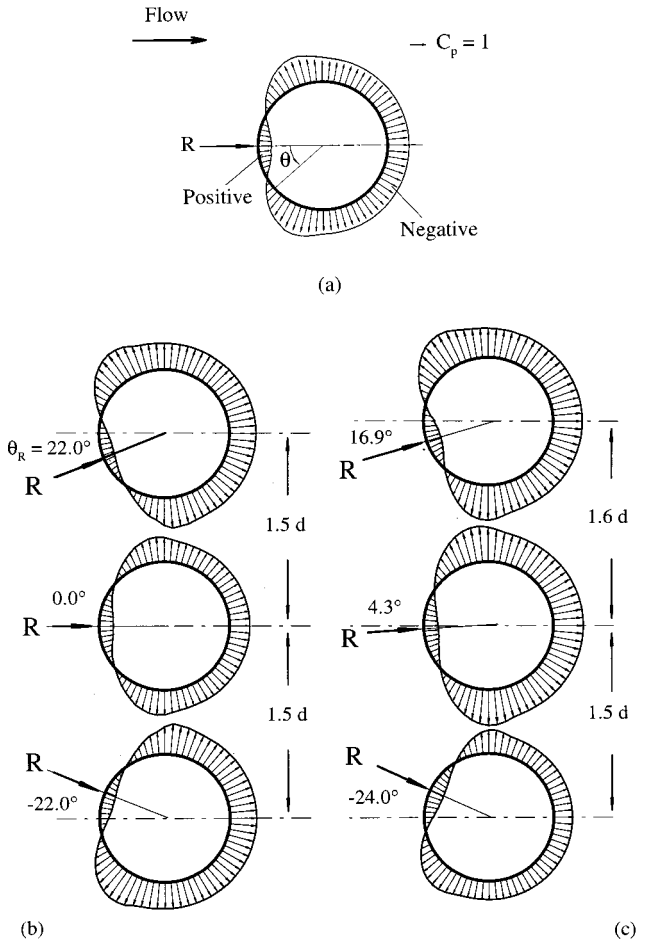

FIG. 2. Polar plots of static pressure C_p around cylinders. The direction of the resultant force is given by $\theta_R=\tan^{-1}(C_L/C_D)$. (a) Single cylinder; (b) three cylinders: $T_1/d=T_2/d=1.5$; and (c) three cylinders: $T_1/d=1.5$, $T_2/d=1.6$.

III. PRESSURE, LIFT, AND DRAG

Figure 2 presents the polar plots of the pressure coefficient $C_p=2\Delta p/(\rho U_\infty^2)$ around the cylinders. Here, Δp is the mean pressure difference between the wall static pressure and a reference pressure and $\theta=0$ corresponds to the forward stagnation point in a single cylinder case [Fig. 2(a)]. Table I lists the base pressure coefficient C_{pb} ($\theta=180°$), the mean drag coefficient C_D ($\equiv 2D/\rho U_\infty^2$, where D is the mean drag force) and lift coefficient C_L ($\equiv 2L/\rho U_\infty^2$, where L is the mean lift force). The table also includes the resultant force direction $\theta_R=\tan^{-1}(C_L/C_D)$ and the forward stagnation point θ_s, identified with the location where the pressure is the maximum.

In the symmetrical arrangement, i.e., at $T_1/d=T_2/d=1.5$ [Fig. 2(b)], the pressure distribution around the upper cylinder appears to be a mirror reflection to that around the lower cylinder. The pressure around the central cylinder is also symmetrical about the flow centerline, i.e., $y/d=0$. Compared with the single cylinder case, C_{pb} drops to -1.49 for the upper and lower cylinders but increases to -1.14 for the central cylinder. However, C_D is identical for the three cylinders. Note that the pressure around each cylinder is quite symmetrical about the stagnation point and θ_R is approximately equal to θ_s, that is, the resultant force on the cylinder is directed approximately through the forward stagnation point and the cylinder center. The observation is the same as the previous reports for a two-cylinder case.[5,18] The angles θ_s of the upper and lower cylinders are 19.4° and $-19.4°$, respectively; the corresponding C_L are 0.48 and -0.48, indicating a repulsive force between the three cylinders. On the other hand, θ_s is zero for the central cylinder and C_L is zero because of the symmetrical pressure distribution about $y/d=0$. It can be inferred that the flow behind the cylinders is symmetrical about $y/d=0$.

TABLE I. Some results of pressure measurements.

		C_D	C_L	θ_R (°)	θ_S (°)	C_{pb}
Single cylinder		0.97	0	0.0	0.0	−1.21
Three cylinders	upper	1.19	0.48	22.0	19.4	−1.49
$T_1/d=T_2/d=1.5$	middle	1.19	0.00	0.0	0.0	−1.14
	lower	1.19	−0.48	−22.0	−19.4	−1.49
$T_1/d=1.5$	upper	1.28	0.39	16.9	16.5	−1.58
$T_2/d=1.6$	middle	1.60	0.12	4.3	4.1	−1.62
	lower	0.92	−0.41	−24.0	−23.5	−1.02

In the asymmetrical arrangement, i.e., $T_1/d=1.5$ and $T_2/d=1.6$ [Fig. 2(c)], the pressure around all three cylinders exhibits a considerable change from the symmetrical arrangement case [Fig. 2(b)]. The pressure around the upper cylinder is no longer a mirror reflection to that around the lower one. The upper cylinder C_{pb} (Table I) is significantly smaller. For the central cylinder, the pressure is asymmetrical about $y/d=0$; θ_s moves away from zero, given by 4.3°. C_{pb} is almost the same as that of the upper cylinder; it reduces significantly, compared with the symmetrical case. However, the pressure around each cylinder appears symmetrical about the forward stagnation point, as the case of $T_1/d=T_2/d=1.5$. Furthermore, θ_s remains nearly the same as θ_R. The angle θ_s is 16.5° for the upper cylinder and −23.5° for the lower one. Accordingly, the upper cylinder C_L is smaller in magnitude, though marginally, than the other. Due to a nonzero θ_s, the central cylinder is associated with a positive C_L. Again, C_L indicates a repulsive force between the cylinders. C_D associated with the central cylinder is largest. In contrast with the case of $T_1/d=T_2/d=1.5$, the flow behind the cylinders will be asymmetrical about $y/d=0$, as confirmed by the cross-flow distributions of the mean velocity and Reynolds stresses and flow visualization data.

Kumada *et al.*[13] measured the flow around three equally spaced side-by-side circular cylinders at Re=(1.0–3.2) $\times 10^4$. At $T/d=1.75$, they observed a symmetric flow, about $y/d=0$, behind the cylinders. The drag associated with the outer two cylinders was larger than that of the central cylinder. At $T/d=1.25$, the flow was asymmetrical and the drag of the central cylinder was larger than that of the two outer cylinders. Similar measurements have been made by Gerhardt and Kramer[19] at Re=10^7. The drag measured presently at $T_1/d=1.5$ and $T_2/d=1.6$ exhibits similar characteristics as theirs at $T/d=1.25$, though it is not clear why the present drag measurement at $T_1/d=T_2/d=1.5$ shows discrepancy from theirs at $T/d=1.75$. Speculatively, this discrepancy may be attributed to a difference in the cylinder spacing between the two measurements.

IV. MEAN VELOCITY, REYNOLDS STRESSES AND SPECTRA

A. Flow behind equally spaced cylinders

Figure 3 presents the cross-stream distributions of the mean velocity $\overline{U}^*$, Reynolds normal stresses $\overline{u^2}^*$, $\overline{v^2}^*$ and Reynolds shear stress $\overline{uv}^*$ at $x/d=2.5$. The overbar denotes time averaging, and the asterisk indicates normalization by U_∞ and d.

At $T_1/d=T_2/d=1.5$, the $\overline{U}^*$, $\overline{u^2}^*$, $\overline{v^2}^*$, and $\overline{uv}^*$ distributions show reasonable symmetry or antisymmetry with respect to $y/d=0$, internally consistent with the pressure distributions. $\overline{U}^*$ [Fig. 3(a)] is significantly negative between $y/d=-0.75$ and 0.75, apparently resulting from the flow reversal. The $\overline{u^2}^*$ distribution [Fig. 3(b)] displays two peaks, which occur near the flow centerline and correspond approximately to the maximum mean velocity gradient. But $\overline{v^2}^*$ does not show peaks at the corresponding location. Instead, $\overline{v^2}^*$ exhibits two peaks at $y/d\approx\pm 2.0$; at the corresponding location, $\overline{U}^*$ displays troughs. The spectra E [Fig. 4(a)] of the single hot-wire data measured at $x/d=2.5$ show two major peaks. The one at $f^*=fd/U_\infty=0.373$ occurs for $y/d\geqslant 2$ and $y/d\leqslant -2$, apparently linked to the peaks in $\overline{v^2}^*$ because of their coinciding lateral locations. The other at $f^*=0.069$ is near the flow centerline and is possibly related

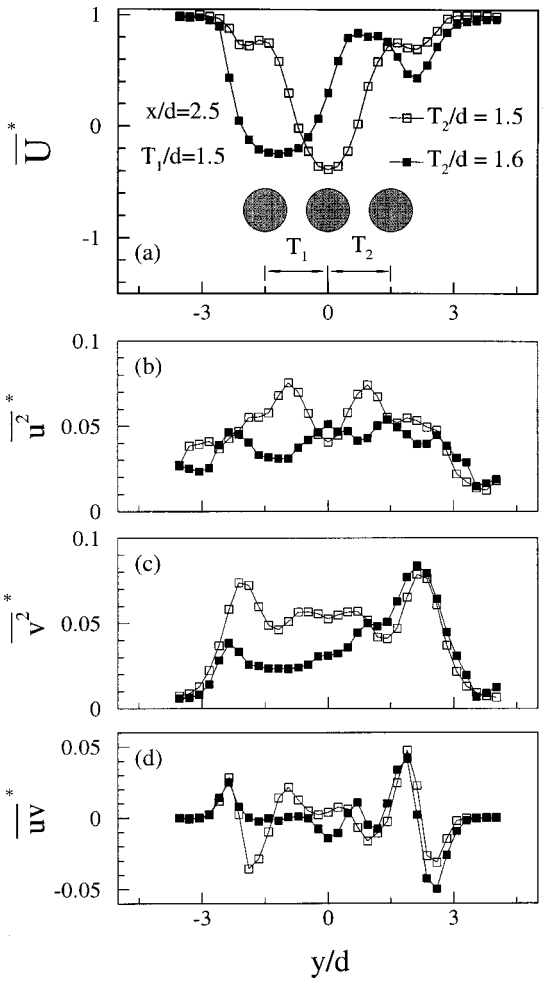

FIG. 3. Lateral distribution of mean velocity, Reynolds normal stresses and shear stress at $x/d=2.5$. □, $T_1/d=T_2/d=1.5$; ■, $T_1/d=1.5$, $T_2/d=1.6$.

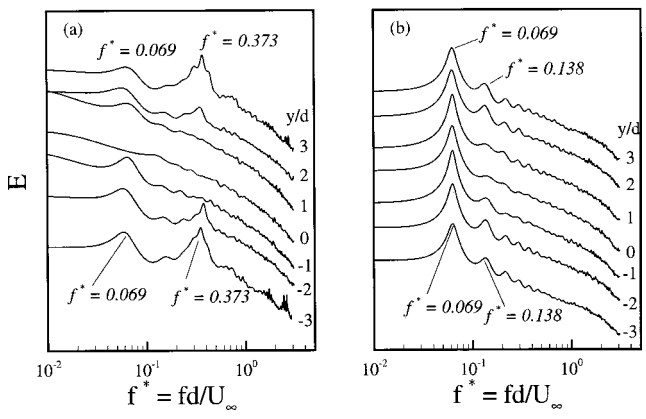

FIG. 4. Power spectra E of single hot-wire signals at $T_1/d=T_2/d=1.5$. (a) $x/d=2.5$; (b) $x/d=10$.

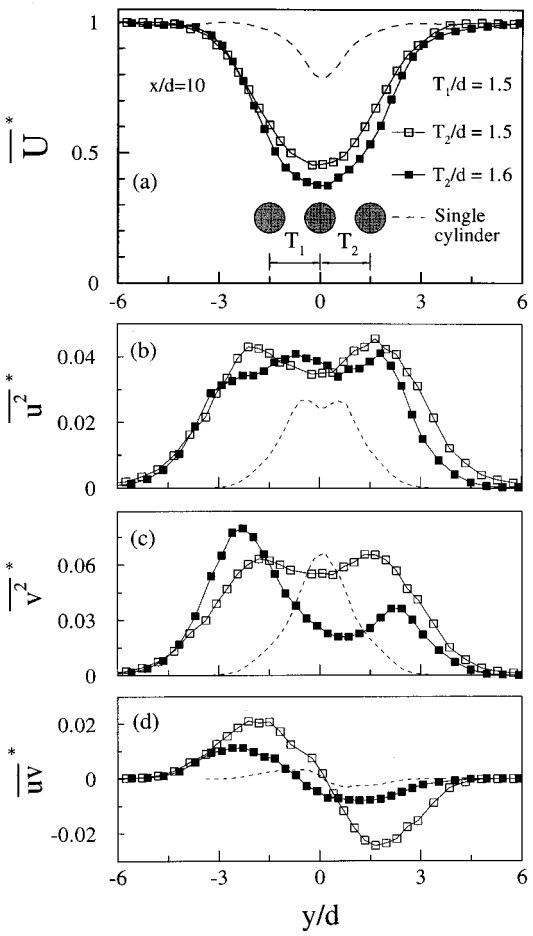

FIG. 5. Lateral distribution of mean velocity, Reynolds normal stresses, and shear stress at $x/d=10$. □, $T_1/d=T_2/d=1.5$; ■, $T_1/d=1.5$, $T_2/d=1.6$.

to the two peaks in $\overline{u^2}^*$. Zhou and Antonia[20] compared the turbulent near-wakes ($x/d=10$) generated by a screen and solid bluff bodies including circular, square, and triangular cylinders. They noted that $\overline{v^2}^*$ was larger than $\overline{u^2}^*$ in the wake of solid bluff bodies. But this was reversed in the screen wake, resembling the case in the turbulent far-wake of a circular cylinder.[21] The observation was related to a difference in the generation mechanisms of vortices. While vortices behind a solid body originated from the vortex shedding, those in a screen near-wake or the far-wake of a solid body were ascribed to the shear layer instability. It seems plausible that the peaks in $\overline{u^2}^*$ are due to vortices generated by the shear layer instability and those in $\overline{v^2}^*$ may result from vortices shed from the free-stream side of the upper and lower cylinders.

The distributions (Fig. 5) of $\overline{U}^*$, $\overline{u^2}^*$, $\overline{v^2}^*$, and $\overline{uv}^*$ at $x/d=10$ are totally different from those at $x/d=2.5$, implying a drastic change in the flow topology. For the purpose of comparison, the single-cylinder data at $x/d=10$ were also measured and included. The single-cylinder data are in reasonable agreement with the previous report,[22] thus providing a validation for the present measurement. The $\overline{U}^*$, $\overline{u^2}^*$, $\overline{v^2}^*$, and $\overline{uv}^*$ distributions behind the three cylinders are qualitatively similar to those of a single cylinder, suggesting

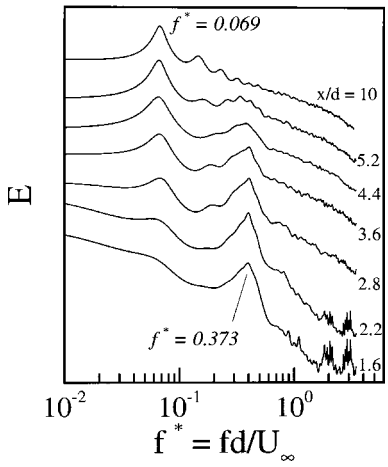

FIG. 6. Power spectra E of hot-wire signals at various downstream stations. $T_1/d=T_2/d=1.5$, $y/d=3$.

a single vortex street. This is confirmed later in Sec. V B by phase-averaged flow pattern. Note that the $\overline{v^2}^*$ profile displays a single peak for the single-cylinder case but a twin-peak for the three cylinders. The twin-peak profile may occur if the two rows of vortical structures have a relatively large lateral spacing. The spectra E [Fig. 4(b)] of the streamwise velocity fluctuation u shows a prominent peak at $f^*=0.069$ across the wake. One minor peak at $f^*=0.138$ is apparently the second harmonic of $f^*=0.069$. This prominent peak indicates the vortex frequency.

It is of interest to note the identification of the same frequency in hot-wire signal spectra at $x/d=2.5$ and 10. Figure 6 presents the spectra of hot-wire signals measured at various downstream stations ($y/d=3.0$). Two major peaks are identifiable. Immediately behind the cylinders, say at $x/d=1.6$ and 2.2, the peak at $f^*=0.373$ is most prominent. As suggested earlier and also verified later, this peak is due to vortices shed from the free-stream side of the upper and lower cylinders. Further downstream, these vortices quickly impair and totally disappear after $x/d=5.2$. On the other hand, the other peak at 0.069 begins with only a faint hump at $x/d=1.6$, but it grows as x/d increases and becomes dominant after $x/d=4.4$. Therefore, the vortical structures corresponding to $f^*=0.069$ do not seem to originate from the shedding process. More discussion on this observation will be made later.

B. Flow behind unequally spaced cylinders

For the asymmetrical arrangement, $\overline{U}^*$, $\overline{u^2}^*$, $\overline{v^2}^*$, and $\overline{uv}^*$ at $x/d=2.5$ (Fig. 3) exhibit a distinct difference from those in the symmetrical arrangement. The flow reversal now occurs largely behind the lower cylinder, as evidenced by a negative $\overline{U}^*$ between $y/d=-2.2$ and -0.3 [Fig. 3(a)]. $\overline{U}^*$ displays a small trough near $y/d=2.2$ and the corresponding $\overline{v^2}^*$ [Fig. 3(c)] shows a relatively strong peak, probably because of vortices shed from the free-stream side of the upper cylinder. Another tiny peak occurs near $y/d=-2.2$ [Fig. 3(c)]. It may be inferred that the flow topology is quite different from that at $T_1/d=T_2/d=1.5$. At $x/d=10$, the asym-

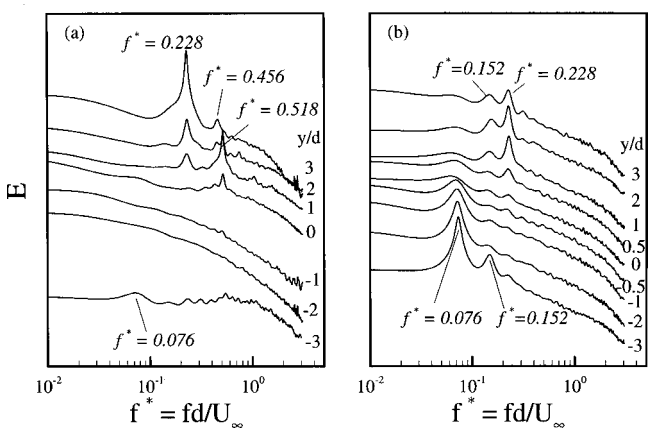

FIG. 7. Power spectra E of single hot-wire signals at $T_1/d=1.5$ and $T_2/d=1.6$. (a) $x/d=2.5$; (b) $x/d=10$.

metry of the Reynolds stresses (Fig. 5) about $y/d=0$ persists. Interestingly, the skewness in the $\overline{v^2}^*$ distribution is reversed, showing one prominent peak at $y/d=-2.2$ and one small peak at $y/d=2.2$. An explanation will be provided in the following in terms of the downstream evolution of the flow topology from $x/d=2.5$ to 10.

In correspondence to the variation in $\overline{U}^*$, $\overline{u^2}^*$, $\overline{v^2}^*$, and $\overline{uv}^*$, the spectra of hot-wire signals also experience an interesting change from $x/d=2.5$ to 10. The spectra E [Fig. 7(a)] of the single hot-wire signals measured at $x/d=2.5$ display one major peak at $f^*=0.228$ for $y/d\geqslant 1$, probably corresponding to the strong peak in $\overline{v^2}^*$ near $y/d=2.2$. The second harmonic of $f^*=0.228$ is also identifiable at $f^*=0.456$. Another peak occurs at $f^*=0.518$ between $y/d\approx 0$ and 2, possibly related to the central cylinder. Again, a tiny hump is discernible at a relatively low frequency $f^*=0.076$ for $y/d=-3$. At $x/d=10$, the peak at $f^*=0.228$ [Fig. 7(b)] is still identifiable for $y/d\geqslant 0$, though significantly weakened. On the other hand, the peak at $f^*=0.076$ is now discernible across the wake, and becomes very prominent for $y/d\leqslant 0$. Its second harmonic of $f^*=0.152$ is also evident.

V. FLOW PATTERNS

A. Flow visualization

At $T_1/d=T_2/d=1.5$, photographs from laser-illuminated flow visualization obtained in the water tunnel are presented in Fig. 8(a). They should be interpreted with

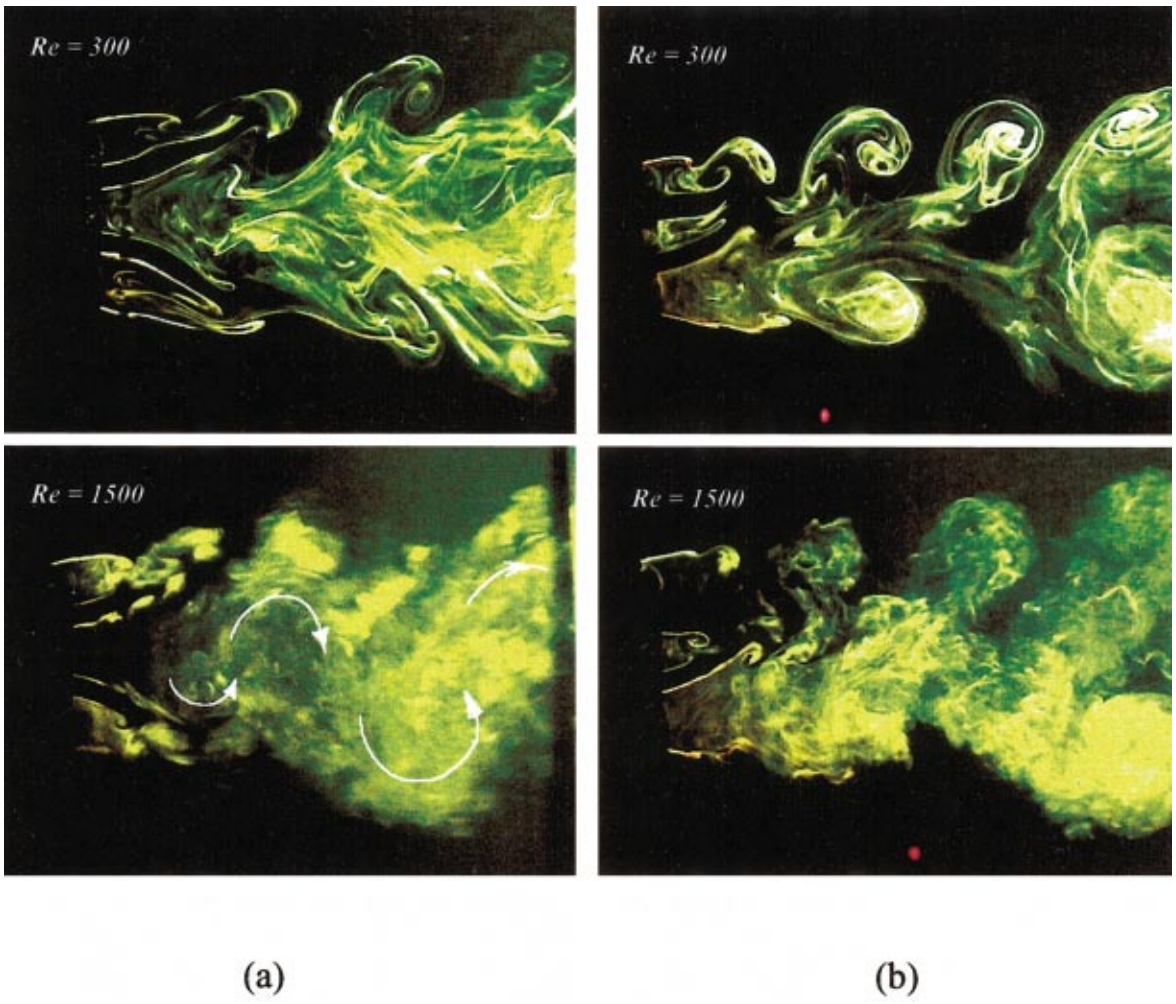

FIG. 8. (Color) Photographs from flow visualization at (a) $T_1/d=T_2/d=1.5$; (b) $T_1/d=1.5$ and $T_2/d=1.6$. Flow is left to right.

caution since the Reynolds number of the flow was considerably smaller than that (Re=5800) in the wind tunnel. Figure 8(a) presents typical photos (Re=300 and 1500). The flow pattern immediately behind the cylinders is symmetrical about the flow centerline, in consistence with the observation from the pressure around cylinders and the cross-stream distributions of the mean velocity and Reynolds stresses. As listed in Table I, the base pressures of the upper and lower cylinders are identical and smaller than that of the central cylinder. Consequently, the two gap flows between cylinders are deflected towards the upper and lower cylinders, respectively, forming a wide wake in the middle and two narrow wakes on either side of the wide wake. The observation is agreeable with previous reports.[8,13]

The present observation of the three-cylinder wake is consistent with Guillaume and LaRue's finding.[15] Guillaume and LaRue obtained three quasi-stable modes of the flow behind three side-by-side cylinders of $T/d=1.338-1.730$. Without any perturbation, the flow structure (their Fig. 9) was the same as that shown in Fig. 8(a). The other two quasi-stable modes occurred, though not always, only after a large perturbation was applied, that is, a wide wake downstream of the upper cylinder or the lower cylinder and two narrow wakes downstream of the other two cylinders. These two modes (not shown) were also observed in the present investigation when the cylinders were installed with the wind tunnel switched on. For example, the wide wake occurred downstream of the lower cylinder if the upper cylinder was last installed. Alternatively, the wide wake was observed downstream of the upper cylinder when the lower cylinder was last installed. Evidently, initial conditions were different in the two occasions. The two modes could occur even by switching off and on the tunnel randomly, which could also correspond to different initial conditions. However, the chance to obtain the two asymmetric modes is much smaller than that for the symmetric mode. It may be concluded that the symmetric mode of the flow structure is most typical behind three side-by-side cylinders of $T_1/d=T_1/d=1.5$, but the two asymmetric wake structures are possible, depending on large perturbations or variation in initial conditions.

Vortex frequencies were estimated by the playback of recorded data and counting consecutive vortices (about 50 pairs) at $x/d\approx 2$ for a certain period. It was found that the vortices were shed at about the same frequency from the upper and lower cylinders. The normalized frequency f_s^* was about 0.373 for Re=450, 0.348, for 1500, and 0.365 for 2000. The blockage effect on the frequency estimate has been corrected. These frequencies are consistent with the occurrence of the peak at $f^*=0.373$ in the spectrum [Fig. 4(a)] considering the experimental uncertainty, estimated to be about 5%, in determining the frequency. It may be concluded that these vortices are probably responsible for the peaks in $\overline{v^{2*}}$ at $y/d\approx\pm 2.0$ [Fig. 3(c)]. In the wide wake, shear layers are seen rolling up, as marked by an arrow in the lower plate of Fig. 8(a), thus forming vortical structures. These structures are likely to be responsible for the peaks in $\overline{u^{2*}}$ near $y/d=\pm 1.0$ [Fig. 3(b)]. By counting consecutive rolling-up vortical structures, the frequency was estimated to be 0.071 for Re=1500 and 0.076 for Re=2000, approximately equal to the frequency $f^*=0.069$, where a peak occurs in the spectrum (Figs. 4 and 6). The observation suggests that the peak may be due to the rolling-up vortical structures in the wide wake.

At $T_1/d=1.5$ and $T_2/d=1.6$, photographs [Fig. 8(b)] from laser-illuminated flow visualization show an asymmetrical flow pattern behind the cylinders, conforming to the observation from the pressure [Fig. 2(c)] around cylinders and the cross-stream distributions of the mean velocity and Reynolds stresses (Fig. 3). As noted in Table I, the central cylinder C_{pb} is considerably smaller than that of lower cylinder, but almost identical to that of the upper cylinder. As a result, the lower gap flow is deflected upwards, while the upper gap flow is not deflected immediately behind the cylinders, forming one wide wake behind the lower cylinder and two narrow wakes behind the central and upper cylinders.

The shear layer appears separated from the central cylinder to form vortices, as indicated in the lower plate of Fig. 8(b) and also by the peak at $f^*=0.518$ in spectra E [Fig. 7(a)]. These vortices, however, quickly break up due to the interactions with the upper narrow wake as well as with the lower wide one so that the peak at $f^*=0.518$ totally disappears from the spectra at $x/d=10$ [Fig. 7(b)].

The vortex shedding from the upper cylinder is evident. The normalized shedding frequency f_s^* was estimated, again by counting consecutive vortices (about 50 pairs) at $x/d\approx 2$ for a certain period, to be 0.211 for Re=1100 and 0.224 for 1500, consistent with the major peak at $f^*=0.228$ in spectra [Fig. 7(a)] when $y/d>0$.

The rolling-up of shear layers is identifiable on the lower side of the wide wake and its frequency is 0.07 for Re =1100 and 0.075 for 1500. Because the rolling-up is limited to a relatively small scale, the spectra E in Fig. 7(a) only display a small hump at $f^*=0.076$ $(y/d=-3)$. The rolling-up structure, however, grows fast in size and in strength [compare Fig. 7(a) with 7(b)] perhaps under the effect of the large mean velocity gradient [Fig. 3(a)]. This explains why the peak at $f^*=0.076$ is so prominent at $x/d=10$ and the reversed skewness in the $\overline{v^{2*}}$ distribution from $x/d=2.5$ [Fig. 3(c)] to 10 [Fig. 5(c)].

B. Phase-averaged flow pattern

In flow visualization experiments, the dye diffuses too fast to be an effective flow marker at $x/d=10$, in particular for the relatively high Reynolds number flow. Therefore, an alternative technique, i.e., the phase-averaging method is used for the study of the flow patterns. Vortices shed from a bluff body are characterized with a marked periodicity. In the near or intermediate wake, a small dispersion is expected in the spanwise spacing, lateral location, strength, and shape of the vortices. The marked periodicity persists even in the presence of neighboring cylinders. Figure 9 illustrates the v-signal from the movable X-wire along with the simultaneously obtained reference v_R-signal from the fixed X-wire at a few typical lateral locations $(T_1/d=T_2/d=1.5)$. A phase relationship is evident between v and v_R signals. As a

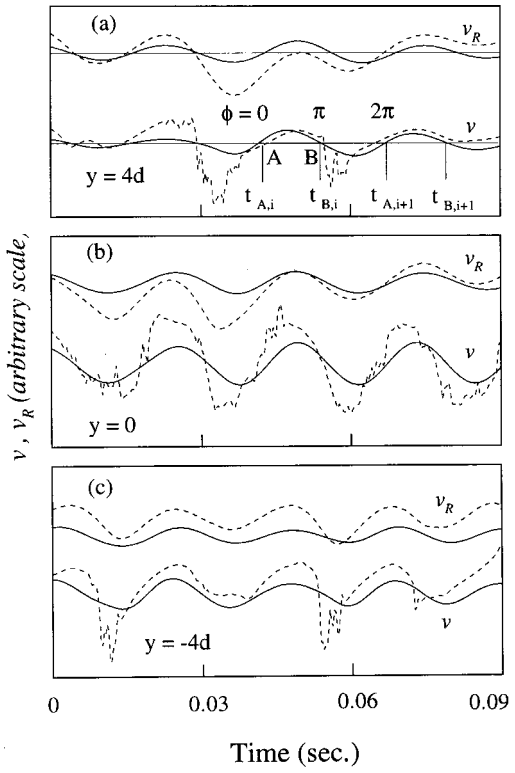

FIG. 9. Signal v from the movable probe and v_R from the reference probe: ---, measured; ———, filtered. (a) $y/d=4$; (b) $y/d=0$; (c) $y/d=-4$. Time=0 is arbitrary, $x/d=10$.

matter of fact, the spectral coherence $Coh_{v_R v}$ ($\equiv \tan^{-1}(Co^2_{v_R v}+Q^2_{v_R v})/E_{v_R}E_v$, where $\mathrm{Co}_{v_R v}$ and $Q_{v_R v}$ are the cospectrum and quadrature spectrum of v_R and v, respectively) reaches almost one at the dominant frequency $f^*=0.069$ for $T_1/d=T_2/d=1.5$ [Fig. 10(a)], indicating a perfect correlation between v_R and v at this frequency. For $T_2/d=1.6$ and $T_1/d=1.5$, $Coh_{v_R v}$ at $f^*=0.076$ is larger than 0.9 for $y/d<0$ [Fig. 10(b)] and remains larger than 0.2 for $y/d>0$. Therefore, the u- and v-signals were phase averaged.

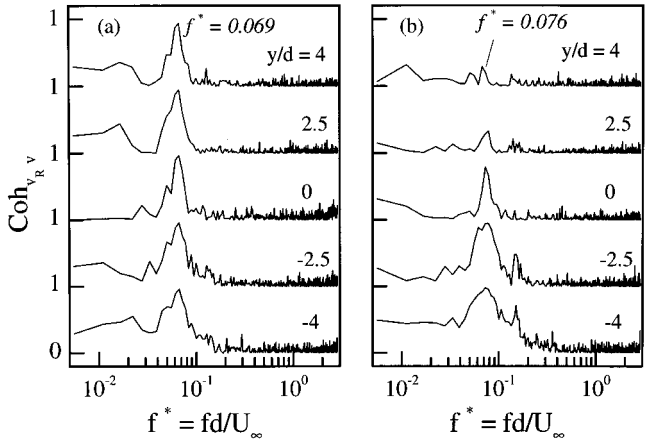

FIG. 10. Spectral coherence between v_R and $v(x/d=10)$. (a) $T_1/d=T_2/d=1.5$; (b) $T_1/d=1.5$, $T_2/d=1.6$.

The phase-averaging method is similar to that used by Matsumura and Antonia[23] and Zhou *et al.*[24] Briefly, the v-signals from the two X-wires were both digitally bandpass filtered with the center frequency set at the dominant vortex frequency, which was identified with $f^*=0.069$ for $T_2/d=T_1/d=1.5$ and $f^*=0.076$ for $T_2/d=1.6$ and $T_1/d=1.5$. Two phases of particular interest were identified on the filtered signal v_f [Fig. 9(a)], i.e.,

$$\text{Phase A: } v_f=0, \text{ and } \frac{dv_f}{dt}>0,$$

$$\text{Phase B: } v_f=0, \text{ and } \frac{dv_f}{dt}<0.$$

The two phases correspond to time $t_{A,i}$ and $t_{B,i}$ (measured from an arbitrary time origin), respectively. The filtered signal from the movable X-wire was used to determine the phase of the u- and v-signals of the movable probe for averaging, viz.

$$\phi=\pi\frac{t-t_{A,i}}{t_{B,i}-t_{A,i}}, \quad t_{A,i}\leqslant t\leqslant t_{B,i},$$

$$\phi=\pi\frac{t-t_{B,i}}{t_{A,i+1}-t_{B,i}}+\pi, \quad t_{B,i}\leqslant t<t_{A,i+1}.$$

The interval between phases A and B was made equal to $0.5T=0.5/f$, where f is the vortex frequency, by compression or stretching; it was further divided into 40 equal intervals. The difference between the local phase at each y-location of the movable X-wire and the reference phase of the fixed X-wire was used to produce phase-averaged sectional streamlines or vorticity contours in the (ϕ,y)-plane.

The phase average of an instantaneous quantity B is given by

$$\langle B\rangle_k=\frac{1}{N}\sum_{i=1}^{N}B_{k,i},$$

where k represents phase. For convenience, the subscript k will be omitted hereafter. N is the number of detected periods, about 800 in the present context.

Figure 11 presents the iso-contours of phase-averaged vorticity and the corresponding sectional streamlines for $T_1/d=T_2/d=1.5$. The phase ϕ, ranging from -2π to $+2\pi$, can be interpreted in terms of a longitudinal distance; $\phi=2\pi$ corresponds to the average vortex wavelength. To avoid any distortion of the physical space the same scales are used in the ϕ- and y-directions in Fig. 11. Vorticity is calculated by

$$\tilde{\omega}=\frac{\partial(\overline{V}+\tilde{v})}{\partial x}-\frac{\partial(\overline{U}+\tilde{u})}{\partial y}\approx\frac{\Delta\tilde{v}}{\Delta x}-\frac{\Delta(\overline{U}+\tilde{u})}{\Delta y},$$

where $\Delta x=-U_c\Delta t=-U_c/f_{\text{sampling}}$. U_c is the average convection velocity of vortices, given by the velocity $\overline{U}+\tilde{u}$ ($=0.653U_\infty$ for $T_1/d=T_2/d=1.5$ and $0.724U_\infty$ for $T_1/d=1.5$ and $T_2/d=1.6$) at the vortex center. The vortex center is identified with the location of the maximum phase-averaged vorticity $\tilde{\omega}_{\max}$, marked by "+" in Fig. 11(a). Both phase-averaged vorticity contours and sectional streamlines

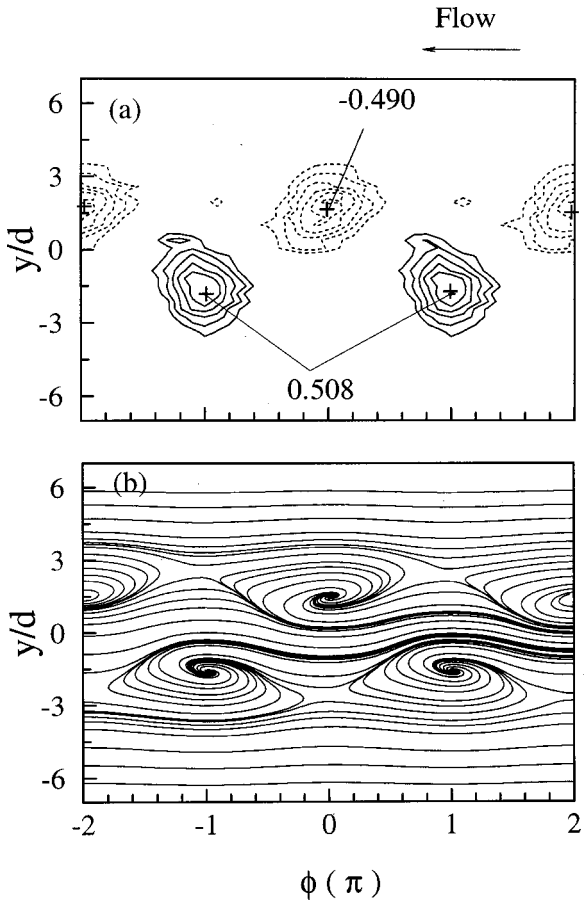

FIG. 11. (a) Phase-averaged vorticity contours $\tilde{\omega}^* = \tilde{\omega} d / U_\infty$ for $T_1/d = T_2/d = 1.5$, contour interval = 0.077; (b) phase-averaged sectional streamlines constructed in a reference frame moving at a velocity $U_c/U_\infty = 0.653$.

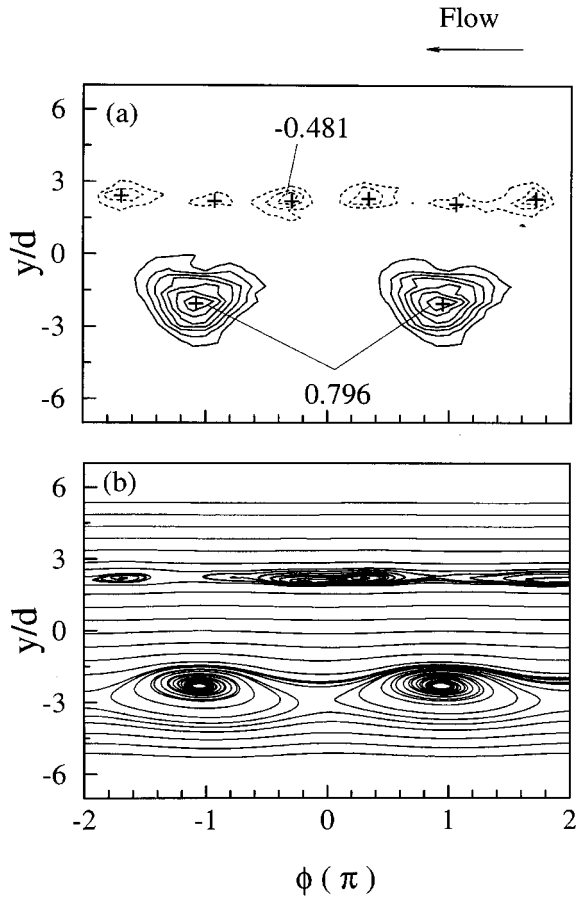

FIG. 12. (a) Phase-averaged vorticity contours $\tilde{\omega}^*$ for $T_1/d = 1.5$ and $T_2/d = 1.6$, contour interval = 0.106; (b) phase-averaged sectional streamlines constructed in a reference frame moving at a velocity $U_c/U_\infty = 0.724$.

exhibit a single Kármán-type vortex street. The vortex frequency is $f^* = 0.069$, the same as the rolling-up frequency of the wide wake, corroborating the suggestion that the vortices at $x/d = 10$ may originate from the rolling-up vortical structures in the wide wake immediately behind the cylinders.

For $T_2/d = 1.6$ and $T_1/d = 1.5$, the phase-averaged vorticity contours [Fig. 12(a)] and sectional streamlines [Fig. 12(b)] show an asymmetrical vortex street with the lower row characterized by large scale and high concentration of vorticity but the upper row characterized by small-scale structures of a higher frequency. The maximum of the phase-averaged vorticity $\tilde{\omega}^* = \tilde{\omega} d / U_\infty$ is about 0.8 for the lower row, higher than that (≈ 0.5) at $T_2/d = T_1/d = 1.5$, probably because the corresponding maximum velocity gradient is larger [refer to Figs. 3(a) and 5(a)].

VI. DISCUSSION

Based on the present measurements, a summary sketch is presented in Fig. 13 of the vortex formation and downstream evolution in each case. At $T_1/d = T_2/d = 1.5$, the flow behind the cylinders is symmetrical about the flow centerline. The base pressures of the upper and lower cylinders are identical but smaller than that of the central cylinder (Table I). Consequently, the gap flows between cylinders are deflected towards the upper and lower cylinders, respectively, forming one wide wake behind the central cylinder and one narrow wake on each side of the wide wake. Vortices are shed from both sides of the upper or lower cylinder at a frequency $f_s^* = 0.373$. These vortices disappear at $x/d \approx 5$ (Fig. 6) probably due to interactions with the wide wake. The dominant frequency in the wide wake is $f^* = 0.069$. The corresponding vortical structures do not appear generated from the shear layer separation from the central cylinder. Photographs from flow visualization indicated that these structures originated from the shear layer rolling-up at about $2d$ or $3d$ downstream from the cylinder, suggesting the shear layer instability to be responsible for their generation. This suggestion is supported by the downstream evolution of the vortex strength. The vortical structures in the wide wake grow in strength downstream (Fig. 6), in marked contrast with those shed from a cylinder whose strength decays as x/d increases.[25] These growing vortical structures form a single staggered vortex street further downstream (Fig. 11).

At $T_1/d = 1.5$ and $T_2/d = 1.6$, the flow shows a remarkable change. A slightly wider upper gap corresponds to an increase in the gap flow velocity, which is supported by the increased $\overline{U}^*$ for $y/d \approx 0.5 \sim 1.5$ [Fig. 3(a)], compared with that at $T_1/d = T_2/d = 1.5$. Correspondingly, the pressure of

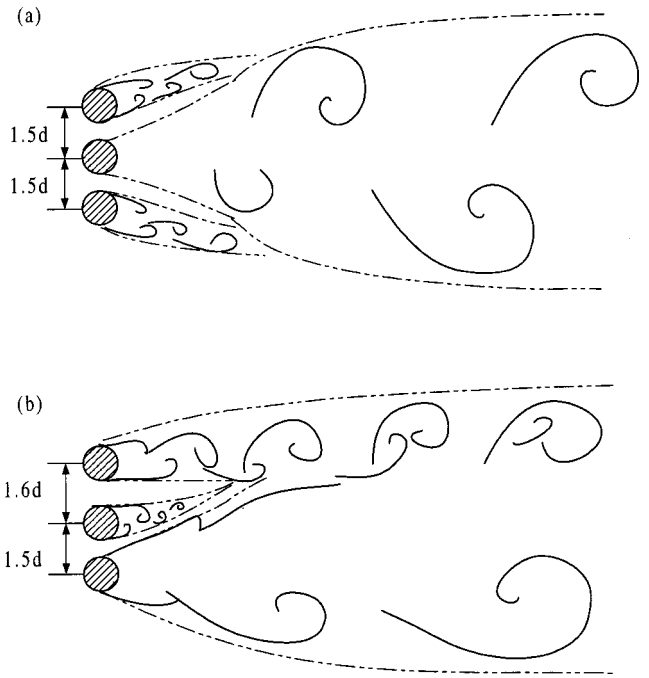

FIG. 13. Summary sketch of the downstream evolution of vortex streets. (a) $T_1/d=T_2/d=1.5$; (b) $T_1/d=1.5$ and $T_2/d=1.6$.

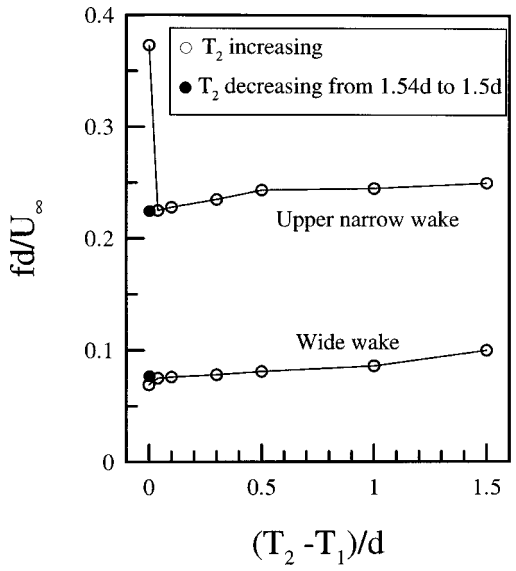

FIG. 14. Variation of the dominant frequencies with the increasing and decreasing of $(T_2-T_1)/d$. $T_1/d=1.5$.

the upper gap flow should decrease, inducing the upward deflection of the lower gap flow. The upward deflected gap flow could subsequently cause the base pressure of the central cylinder to drop, compared with that at $T_1/d=T_2/d=1.5$, to a level almost the same as that of the upper cylinder (Table I). As a result, the upper gap flow is no longer deflected [Fig. 8(b)] and we see two narrow wakes behind the upper and central cylinders, respectively, and one wide wake behind the lower cylinder. The vortex shedding is identifiable in the two narrow wakes and its frequency is $f_s^*=0.228$ for the upper cylinder and 0.518 for the central cylinder, as determined from the hot-wire signal spectrum and also verified by counting vortices for a period from flow visualization data. In the wide wake, the shear layer starts to roll-up near $x/d=2$ at a frequency of $f^*=0.076$. It is pertinent to mention that tests have been conducted to adjust the cylinder spacing from $T_1/d=T_2/d=1.5$ to $T_1/d=1.5$ and $T_2/d=1.54$. (The uncertainty to determine cylinder spacing was estimated to be 0.5 mm or $0.04d$, mainly due to the curvature of cylinders.) In response to this change the flow changed from the symmetric to the asymmetric mode. However, when unequal cylinder spacing ($T_1/d=1.5$ and $T_2/d=1.54$) was gently changed to equal cylinder spacing ($T_1/d=T_2/d=1.5$), the symmetric mode of the flow could not be recovered. A further increase in T_2/d results in only a slight change in the vortex frequencies, as presented in Fig. 14 for the vortex frequencies in the upper narrow wake and the wide wake. The frequency $f^*=0.076$ is marginally larger than that (0.069) at $T_2/d=T_1/d=1.5$. Roshko[26] proposed a universal Strouhal number $\mathrm{St}_u=f_s d_w/U_w$, where d_w is the wake width and $U_w=U_\infty(1-C_{pw})^{1/2}$, where C_{pw} is the pressure in the wake. St_u is a constant, about 0.16 in a single cylinder wake. The Strouhal number St was then written as $\mathrm{St}=\mathrm{St}_u(d/d_w)(1-C_{pw})^{1/2}$. Evidently, d_w or the shear layer thickness and St are inversely related. Presumably, this relationship is also applicable for the vortical structures generated by the shear layer instability. Then the slight increase in f^* may be attributed to a decrease in the shear layer thickness, which is deducible from the $\overline{U}^*$ distributions [Fig. 3(a)]. The corresponding vortical structures again grow in strength when moving downstream. This is evident when comparing the spectra at $x/d=2.5$ [Fig. 7(a)] and those at $x/d=10$ [Fig. 7(b)]. The vortices shed from the central cylinder vanish quickly probably due to their weak strength and interactions with the growing lower wide wake; the interaction with the upper narrow wake is likely to play a minor role only in their vanishment [see Fig. 8(b)]. The vortices in the upper narrow wake survive longer, possibly because of a relatively weak interaction with the wide wake, than those in the narrow wakes at $T_2/d=T_1/d=1.5$. The above discussion is consistent with the phase-averaged flow pattern at $x/d=10$, which display an asymmetrical vortex street. The lower row vortical structures of a frequency $f^*=0.076$ are characterized by a larger size and higher vorticity concentration than those of the upper row, which retain the frequency when shedding, i.e., $f_s^*=0.228$.

A remark is due here on the difference in the gap flows between three- and two-cylinder configurations. In both situations, the gap flows are generally deflected. However, the deflected gap flows in the three-cylinder case are quasi-stable, whether the cylinder spacing is equal or not; the change in the deflection direction is not observed. The change, however, can be caused by large perturbations, as reported by Guillaume and Larue,[15] variation in initial conditions (Sec. V A) and unequal cylinder spacing. On the other hand, the gap flow deflection is bi-stable in the two side-by-side cylinder arrangement ($T/d\approx 1.2-2.2$), and spontaneously changes over in a random manner from one side to another.[4,5] Time scale for the change-over is several orders of magnitude longer than that of vortex shedding and

also several orders of magnitude longer than that for the instability of the separated shear flows.[7] The bi-stable gap flow is well known but the mechanism is not well understood. We have seen in the three-cylinder case that a slight inequality in cylinder spacing, e.g., $T_1/d=1.5$ and $T_2/d=1.6$, leads to a remarkable change in the pressure field and hence the reorientation of both gap flows. The vortex shedding process is associated with a fluctuation in both velocity and pressure fields. This fluctuation is likely to be responsible for inducing the initial gap flow deflection. Presumably, the deflected gap flow is associated with a relatively high momentum. As a result, the base pressure behind the cylinder, towards which the gap flow is deflected, should be low and that behind the other cylinder, where fluid has a relatively low momentum, should be high. In addition, the vortices shed from the cylinder in the narrow wake are generally characterized by a high frequency and perhaps relatively weak strength. Those generated from the shear layer rolling-up in the wide wake could be even weaker (Fig. 4). Therefore, the fluctuation of the velocity or pressure field could have a limited strength, generally not strong enough to force the gap flow to change over from one side to another. However, the nonlinear interaction between the two wakes may generate a rather large fluctuation of the pressure field from time to time and tip the balance, causing the change-over of the gap flow deflection. In the three-cylinder case, both of the deflected gap flows act to maintain the high base pressure behind the central cylinder. It is more difficult to tip the balance. Consequently, the flow field is quasi-stable.

It is worthwhile commenting on the phase relationship between the vortex streets behind upper and lower cylinders for $T_1/d=T_2/d=1.5$. In order to monitor vortex shedding from the free-stream side of upper and lower cylinders, measurements were conducted with two hot wires placed at $x/d=2$ and $y/d=\pm 3.0$, respectively. The spectral phase angle[27] [Fig. 15(a)] at $f_s^*=0.373$ between the hot-wire signals obtained at $y/d=\pm 3.0$ is near $-\pi$, suggesting a predominantly in-phase relationship between the two external streets. This phase relation is also observed downstream at $x/d=10$ and $y/d=\pm 5.5$ [Fig. 15(b)], which is internally consistent with the staggered arrangement of vortices (Fig. 11). However, the in-phase relationship between the two external streets at $x/d=2$ is not necessarily related to the staggered arrangement of vortices at $x/d=10$ since the two external streets vanish at $x/d\approx 5$, as indicated in Figs. 6 and 8(a). The phase relationship between the two external streets for $T_1/d=1.5$ and $T_2/d=1.6$ was not measured because the two streets are characterized by different vortex frequencies.

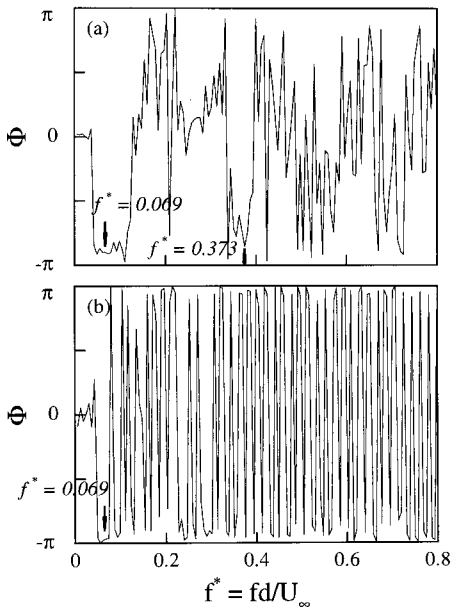

FIG. 15. Spectral phase Φ between velocity signals measure at (a) $y/d=\pm 3$, $x/d=2$; (b) $y/d=\pm 5.5$, $x/d=10$. $T_1/d=T_2/d=1.5$.

VII. CONCLUSIONS

The effect of unequal cylinder spacing on the vortex streets behind the three side-by-side cylinders has been investigated. A slight inequality between T_1/d and T_2/d can lead to a substantial change in the pressure distribution about the cylinders. Subsequently, the drag and lift on the cylinders are different from those at $T_1/d=T_2/d=1.5$. In each case, however, the resultant force on each cylinder is directed approximately through the forward stagnation point and the cylinder center, as previously reported in a two-cylinder case.[5,18]

There is a remarkable change in the vortex formation, flow patterns, and downstream evolution. At $T_1/d=T_2/d=1.5$, the flow is symmetrical about the flow centerline, showing one wide wake behind the central cylinder and two narrow wakes behind the upper and lower cylinders. Further downstream at $x/d=10$, a single vortex street occurs. The flow may change from the symmetric to the asymmetric mode due to a large flow perturbation, variation in initial condition, and slight cylinder spacing, but not vice versa. At $T_1/d=1.5$ and $T_2/d=1.6$, the lower gap flow is deflected upwards but the upper one is not deflected, forming a wide wake behind the lower cylinder and two narrow wakes behind the other two cylinders. The narrow wake behind the central cylinder disappears at $x/d\approx 5$, resulting in one single asymmetrical vortex street further downstream.

The dominated frequency is $f^*=0.373$ in the narrow wakes and 0.069 in the wide wake for $T_1/d=T_2/d=1.5$. This frequency is 0.228 in the upper narrow wake, 0.518 in the middle narrow wake, and 0.076 in the wide wake for $T_1/d=1.5$ and $T_2/d=1.6$. In both cases, the vortical structures in the wide wake are generated probably due to the shear layer instability; they grow in strength up to $x/d\approx 5$ and have a strong presence at $x/d=10$. In contrast, those in the narrow wakes originate from the vortex shedding from cylinders and disappear quickly, probably due to the interactions with the wide wake. The upper narrow wake in the case of $T_1/d=1.5$ and $T_2/d=1.6$ is exceptional. The vortical structures appear to interact weakly with the wide wake; they are identifiable at $x/d=10$.

ACKNOWLEDGMENT

Y. Z. wishes to acknowledge support given to him by the Research Grants Council of the Government of the Hong Kong Special Administrative Region through Grant No. PolyU5161/97E.

[1]M. M. Zdravkovich, ''Review of flow interference between two circular cylinders in various arrangements,'' J. Fluids Eng. **99**, 618 (1977).
[2]L. Landweber, ''Flow about a pair of adjacent, parallel cylinders normal to a stream,'' D. W. Taylor Model Basin, Department of the Navy, Report 485, Washington, D.C. (1942).
[3]H. M. Spivac, ''Vortex frequency and flow pattern in the wake of two parallel cylinders at varied spacings normal to an air stream,'' J. Aeronaut. Sci. **13**, 289 (1946).
[4]S. Ishigai, E. Nishikawa, K. Nishmura, and K. Cho, ''Experimental study on structure of gas flow in tube banks with tube axes normal to flow (Part I, Kármán vortex flow around two tubes at various spacings),'' Bull. JSME **15**, 949 (1972).
[5]P. W. Bearman and A. J. Wadcock, ''The interference between a pair of circular cylinders normal to a stream,'' J. Fluid Mech. **61**, 499 (1973).
[6]C. H. K. Williamson, ''Evolution of a single wake behind a pair of bluff bodies,'' J. Fluid Mech. **159**, 1 (1985).
[7]H. J. Kim and P. A. Durbin, ''Investigation of the flow between a pair of circular cylinders in the flopping regime,'' J. Fluid Mech. **196**, 431 (1988).
[8]D. Sumner, S. S. T. Wang, S. J. Price, and M. P. Paidoussis, ''Fluid behavior of side-by-side circular cylinders in steady cross-flow,'' J. Fluids Struct. **13**, 309 (1999).
[9]Y. Zhou, R. M. C. So, M. H. Liu, and H. J. Zhang, ''Complex turbulent wakes generated by two and three side-by-side cylinders,'' Int. J. Heat Fluid Flow **21**, 125 (2000).
[10]M. M. Zdravkovich and K. L. Stonebanks, ''Intrinsically nonuniform and metastable flow in and behind tube arrays,'' J. Fluids Struct. **4**, 305 (1990).
[11]P. M. Moretti, ''Flow-induced vibrations in arrays of cylinders,'' Annu. Rev. Fluid Mech. **25**, 99 (1993).
[12]P. Le Gal, I. Peschard, M. P. Chauve, and Y. Takeda, ''Collective behavior of wakes downstream of a row of cylinders,'' Phys. Fluids **8**, 2097 (1996).
[13]M. Kumada, M. Hiwada, M. Ito, and I. Mabuchi, ''Wake interference between three circular cylinders arranged side by side normal to a flow,'' Trans. Jpn. Soc. Mech. Eng., Ser. B **50**, 1699 (1984) (in Japanese).
[14]M. Hayashi, A. Sakurai, and Y. Ohya, ''Wake interference of a row of normal flat plates arranged side by side in a uniform flow,'' J. Fluid Mech. **164**, 1 (1986).
[15]D. W. Guillaume and J. C. LaRue, ''Investigation of the flopping regime with two-, three- and four-cylinder arrays,'' Exp. Fluids **27**, 145 (1999).
[16]M. D. Palmer and J. F. Keffer, ''An experimental investigation of an asymmetrical turbulent wake,'' J. Fluid Mech. **53**, 593 (1972).
[17]D. Sumner, S. J. Price and M. P. Païdoussis, ''Flow-pattern identification for two staggered circular cylinders in cross-flow,'' J. Fluid Mech. **411**, 263 (2000).
[18]Y. Zhou, Z. J. Wang, R. M. C. So, S. J. Xu, and W. Jin, ''Free vibrations of two side-by-side cylinders in a cross flow,'' J. Fluid Mech. **443**, 197 (2001).
[19]H. J. Gerhardt and C. Kramer, ''Interference effects for groups of stacks,'' J. Wind. Eng. Ind. Aerodyn. **8**, 195 (1981).
[20]Y. Zhou and R. A. Antonia, ''Effect of initial conditions on vortices in a turbulent near wake,'' AIAA J. **32**, 1207 (1994).
[21]Y. Zhou, R. A. Antonia, and W. K. Tsang, ''The effect of the Reynolds number on a turbulent far-wake,'' Exp. Fluids **25**, 118 (1998).
[22]Y. Zhou and R. A. Antonia, ''Critical points in a turbulent near-wake,'' J. Fluid Mech. **275**, 59 (1994).
[23]M. Matsumura and R. A. Antonia, ''Momentum and heat transport in the turbulent intermediate wake of a circular cylinder,'' J. Fluid Mech. **250**, 651 (1993).
[24]Y. Zhou, H. J. Zhang, and M. W. Yiu, ''The turbulent wake of two side-by-side circular cylinders,'' J. Fluid Mech. (to be published).
[25]Y. Zhou and R. A. Antonia, ''A study of turbulent vortices in the wake of a cylinder,'' J. Fluid Mech. **253**, 643 (1993).
[26]A. Roshko, ''On the drag and shedding frequency of bluff cylinders,'' Nat. Adv. Comm. Aero., Washington, Tech. Note 3169 (1954).
[27]R. A. Antonia, Y. Zhou, and M. Matsumara, ''Spectral characteristics of momentum and heat transfer in the turbulent wake of a circular cylinder,'' Exp. Therm. Fluid Sci. **6**, 371 (1993).